A Digital Predistortion for Concurrent Dual-Band Power Amplifier Linearization Based on Periodically Nonuniform Sampling Theory

Siqi Wang, Wenhui Cao, Rui Hou, Thomas Eriksson

A Digital Predistortion for Concurrent Dual-Band Power Amplifiers Linearization Based on Periodically Nonuniform Sampling Theory

Siqi Wang, Wenhui Cao, Rui Hou, Thomas Eriksson

***Abstract*—In this paper, we propose a novel technique of digital predistortion (DPD) for dual-band power amplifiers (PA) based on periodically nonuniform sampling (PNS) theory. In contrast to conventional 2D-DPD models, the proposed PNS-DPD has only a single input which can largely reduce the model complexity. We fold the two stimuli with aliasing and feed it to a simple single-band DPD model. The desired predistorted signals are reconstructed from aliased DPD output through the PNS theory. Compared with conventional multi-input models which include numerous intermodulation products of the input signals, the complexity of the proposed single-input PNS-DPD model is hugely decreased. The model coefficients of the proposed PNS-DPD can be easily extracted with conventional direct or indirect learning architecture. We experimentally evaluate the proposed DPD on a test bench and compare it with other DPD techniques in the literature. The implementation complexity can be reduced by over 30% and the identification complexity is also largely reduced.**

***Index Terms*—Digital predistortion, dual-band, nonlinearity, periodic nonuniform sampling, power amplifiers**

I. Introduction

HUGE number of users need to be connected simultaneously to the modern wireless communication systems, e.g. 5G and beyond [1]. Massive multiple-input multiple-output (MIMO) technology is emerging for the compatibility of different standards which occupy different frequency bands [2]. Carrier aggregation helps to fully utilize the spectrum resources, which however increases the bandwidth of the signal especially when the carriers are not contiguous. Concurrent multi-band power amplifiers (PA) enable transmission of signals for users at different frequency component carriers.

The radio-frequency (RF) PA consumes a large part of the total power in the system. Further, it brings nonlinearity and memory effects, which distorts the transmitted signals. Digital predistortion (DPD) is one of the most commonly used methods to linearize the PA and to enhance its power efficiency [3]. Different DPD models have been developed based on Volterra series, such as memory polynomial (MP) [4], generalized memory polynomial (GMP) [5], dynamic-deviation-reduction (DDR) model [6], and decomposed vector rotation (DVR) model [7]. Block-oriented non linear (BONL) systems [8] have also been studied. Though these single-band DPD models exhibit good linearization performance with a considerable complexity, they need high sampling rate for implementation if we consider the transmitted multi-band signal as a wide band signal. For digital signal processors (DSP) and analog-to-digital converters (ADC), the sampling frequency is a crucial limitation [9]. Since the power consumption of the DPD is related to its sampling rate [10], it is fastidious to process a non-contiguous carrier aggregated signal as a wideband signal.

Concurrent linearization techniques have been developed to reduce the impact of frequency separation between the non-contiguous carriers [11]. A dual-band DPD (2D-DPD) based on MP model has been proposed in [12] to focus only on distortions in the transmission bands. The signals of each carrier are processed individually and they are sampled at a rate which is related to their bandwidths. The input signals of the DPD are the signals of each band filtered out within a small bandwidth. Thus the DPD can be implemented with a low sampling rate. The intermodulation (IMD) effects have been considered in this 2D-DPD by introducing products of the two signals. In [13], a generalized 2D-DPD structure has been analyzed. The GMP and DVR models can be also extended to 2D version for better linearization performance of dual-band transmission as in [14] and [15] respectively. Though these models tremendously reduce the sampling rate compared with the conventional single wideband DPD, their multiple inputs lead to a non-negligible increase of model complexity by including the IMDs. The number of model coefficients concerns not only the DPD power consumption but also the identification accuracy when the length of dataset for model identification has a constraint.

As discussed above, a single-input wide-band DPD (WB-DPD) for multi-band linearization has advantages on model complexity and identification complexity, while the advantage of a multi-band DPD is the lower sampling rate. Periodically nonuniform sampling (PNS) theory [16] provides possibilities to render the DPD with both low complexity and low sampling rate. This PNS procedure can be regarded as decimating a high-rate signal in multiple channels with delays between them. According to the PNS theory, a high-rate signal can be reconstructed from its periodically nonuniform sampled decimated signals. In [17], authors have given the Volterra series with polyphase representations at lower sampling rate. This technique has been used in [18] for DPD identification to reduce the sampling rate of the feedback path. In [19],

Siqi Wang and Thomas Eriksson are with the Department of Electrical Engineering, Chalmers University of Technology, SE-412 96 Gothenburg, Sweden (siqiw@chalmers.se, thomase@chalmers.se).

Wenhui Cao and Rui Hou are with Ericsson AB, Stockholm, Sweden (wenhui.cao@ericsson.com, rui.hou@ericsson.com).

Color versions of one or more of the figures in this paper are available online at http://ieeexplore.ieee.org.

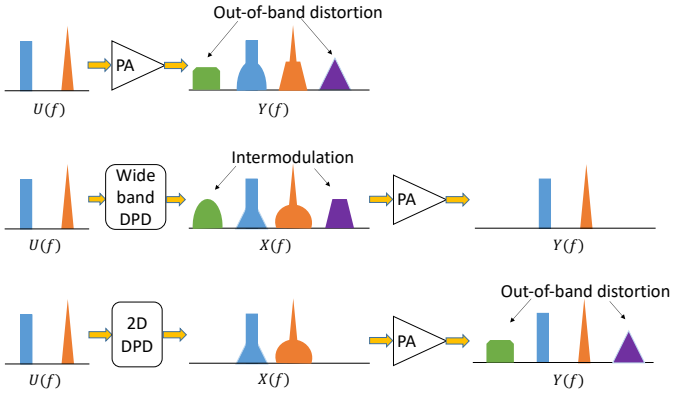

Fig. 1. Spectral expansion by PA and DPD for dual-band signal.

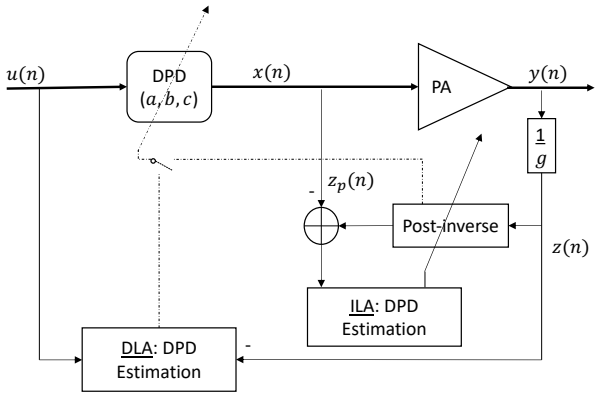

Fig. 2. Conventional single-band DPD and its identification using direct and indirect learning architecture (DLA/ILA).

the PNS technique was used to reconstruct a wide-band signal and a band-limited DPD based on polyphase technique has been proposed. In [20], the PNS technique was proved compatible for multi-band signal reconstruction. The multi-band signal can thus be sampled with low rate thanks to its sparsity in frequency domain. Thus M band-limited signals can be sampled at a low sampling rate which is equal to their bandwidth and then be reconstructed by a group of M delayed low rate signals.

In this paper, we propose a periodically nonuniform sampled DPD (PNS-DPD) for dual-band transmission, which uses a simple single-input model as WB-DPD but runs at low sampling rate as multi-band DPD. With conventional reconstruction theorem in [20], 4 channels are needed for the PNS in the DPD structure. Thanks to the symmetry of frequency locations of IMDs for a dual-band signal, our proposed PNS-DPD needs only 3 channels, which further reduces 25% complexity. The identification of the proposed PNS-DPD is as simple as for the conventional narrow-band DPD with only one feedback path at low sampling rate, and it can be implemented using either the direct or indirect learning architecture (DLA/ILA). According to experimental evaluation on the WebLab testbench [21], the proposed method reaches the same linearization performance but with lower sampling rate and model complexity compared with other conventional methods in the literature.

This paper is organized as follows. Section II presents the conventional high-rate wideband DPD and 2-D DPD. The PNS reconstruction technique is explained in Section III. The details of the proposed PNS-DPD is then described in Section IV. In Section V, the test bench and the corresponding experimental results are presented and discussed. Finally, the conclusion is given in Section VI.

II. Conventional DPD methods for dual-band signal transmission

The conventional ideas of concurrent dual-band linearization can be categorized into two types: one is to consider the transmitted dual-band signal as a single wideband signal and to process with a normal single-band transmission DPD, which is denoted by wideband DPD (WB-DPD); the other is to focus on the distortion compensation in the bands of transmitted signals, which is denoted by dual-band DPD (2D-DPD).

We denote the stimulus as U, the input and output of the PA by X and Y respectively. As illustrated in Fig. 1, the PA generates intermodulation of the two signals and also distortion in each band. As a consequence of that the WB-DPD exhibits the inverse characteristics of the PA, the predistorted signal has also intermodulation at the same frequencies [11]. The PA output Y is very close to the stimulus U after linearization with WB-DPD. The 2D-DPD predistorts only the signals in the transmission bands and the intermodulation is not compensated for as shown in Fig. 1.

A. High rate wideband DPD (WB-DPD)

The dual-band signal can be considered as a single wide-band signal which spreads in a large frequency interval but has a very low occupancy ratio of the useful signal. Since the bandwidth of the signal is large, the required sampling rate of the DPD is correspondingly high.

We use the GMP model for WB-DPD in this paper since it can reach good trade-off between linearization performance and complexity according to [22] [23]. Other models can also be used for the proposed PNS-DPD. If we denote the input and output of the DPD by $u(n)$ and $x(n)$ respectively, their relation can be represented by GMP as [5]:

$$\begin{aligned} x(n) = &\sum_{k=0}^{\mathcal{K}_a-1}\sum_{l=0}^{\mathcal{L}_a-1} a_{kl}u(n-l)|u(n-l)|^k \\ &+\sum_{k=1}^{\mathcal{K}_b}\sum_{l=0}^{\mathcal{L}_b-1}\sum_{m=1}^{\mathcal{M}_b} b_{klm}u(n-l)|u(n-l-m)|^k \\ &+\sum_{k=1}^{\mathcal{K}_c}\sum_{l=0}^{\mathcal{L}_c-1}\sum_{m=1}^{\mathcal{M}_c} c_{klm}u(n-l)|u(n-l+m)|^k \end{aligned} \quad (1)$$

where k is the index for nonlinearity, and l, m are the indices for memory. a_{kl}, b_{klm}, c_{klm} are the complex coefficients of the signal and envelope, the signal and lagging envelope, and the signal and leading envelope, respectively. $\mathcal{K}_a$, $\mathcal{K}_b$, $\mathcal{K}_c$ are the highest orders of nonlinearity. $\mathcal{L}_a$, $\mathcal{L}_b$, $\mathcal{L}_c$ are the highest memory depths. $\mathcal{M}_b$, $\mathcal{M}_c$ denote the longest lagging and leading delay tap length, respectively.

The model coefficients can be estimated using both direct or indirect learning architecture (DLA/ILA) [24] as depicted

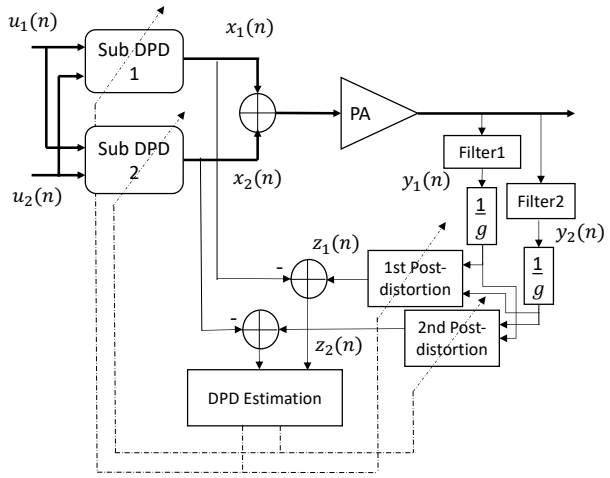

Fig. 3. Conventional dual-band DPD and its identification using ILA.

in Fig 2. A post-inverse of the PA is identified and used as a DPD upstream of the PA. Its input signal is $z(n)$ which is the PA output $y(n)$ divided by g, the gain of PA [25].

Using the ILA, the model coefficients $[a_{kl},\ b_{klm},\ c_{klm}]$ can be estimated by minimizing the difference between the output z_p of the postdistorter and the input x of the PA: $|\epsilon(n)|^2 = |z_p(n) - x(n)|^2$. We use the least square (LS) [26] to estimate the model coefficients

$$\hat{\boldsymbol{c}} = [\mathbf{Z}^H\mathbf{Z}]^{-1}\mathbf{Z}^H\boldsymbol{x}. \tag{2}$$

B. Conventional dual-band DPD (2D-DPD)

In order to reduce the sampling rate of the dual-band signal which has a large frequency separation, dual-band DPD has been proposed to focus on processing the two band signals regardless of their separation. The conventional dual-band DPD processes the signals in two bands individually as depicted in Fig. 3. Each sub DPD has two separate inputs: the lower and upper band signals are denoted by $u_1(n)$ and $u_2(n)$ respectively. The predistorted signal of the i-th DPD is denoted by $x_i(n)$ and can be expressed in function of $u_1(n)$ and $u_2(n)$ by 2-D GMP model [14]:

$$\begin{aligned} x_i(n) = & \sum_{k=0}^{\mathcal{K}_a-1}\sum_{j=0}^{k}\sum_{l=0}^{\mathcal{L}_a-1} a_{kjl}^{(i)} u_i(n-l) \\ & \times |u_i(n-l)|^{k-j}|u_{3-i}(n-l)|^j \\ & + \sum_{k=1}^{\mathcal{K}_b}\sum_{j=0}^{k}\sum_{l=0}^{\mathcal{L}_b-1}\sum_{m=1}^{\mathcal{M}_b} b_{kjlm}^{(i)} u_i(n-l) \\ & \times |u_i(n-l-m)|^{k-j}|u_{3-i}(n-l-m)|^j \\ & + \sum_{k=1}^{\mathcal{K}_c}\sum_{j=0}^{k}\sum_{l=0}^{\mathcal{L}_c-1}\sum_{m=1}^{\mathcal{M}_c} c_{kjlm}^{(i)} u_i(n-l) \\ & \times |u_i(n-l+m)|^{k-j}|u_{3-i}(n-l+m)|^j \\ & = f_i(u_1(n), u_2(n)) \end{aligned} \tag{3}$$

which is similar to the GMP representation (1).

The model coefficients of each sub-DPD can be estimated using ILA as well as illustrated in Fig. 3. The feedback signals

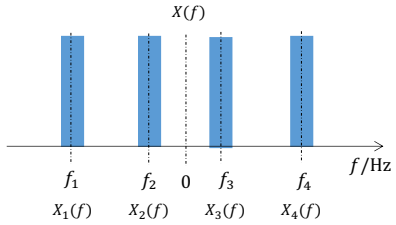

Fig. 4. Spectrum of 4-band signal in baseband.

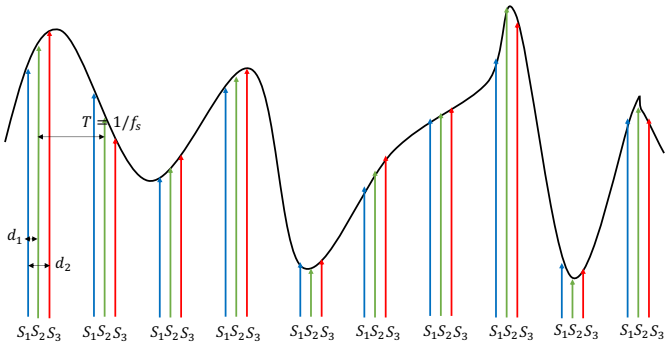

Fig. 5. Periodic nonuniform sampling [PNS(3)].

$y_1(n)$ and $y_2(n)$ are filtered from the PA output within the corresponding frequency band.

We first construct a basis matrix $\boldsymbol{\Psi}_i$ for the i-th band containing the basis functions as described in (3). The coefficients of the i-th band model can then be estimated by solving a linear problem similar to (2) by replacing $\mathbf{Z}$ and $\boldsymbol{x}$ with $\boldsymbol{\Psi}_i$ and $\boldsymbol{x_i}$.

The advantage of 2D-DPD compared with WB-DPD is the lower sampling rate. However the number of coefficients in the 2D-DPD model can be highly increased. As we can see in (3), the number of 2D-DPD coefficients increases in order of $\mathcal{O}(\mathcal{K}^2)$ while the number of 1D-DPD coefficients in (1) is in order of $\mathcal{O}(\mathcal{K})$.

III. PNS RECONSTRUCTION THEOREM

With a single input, the model structure of a WB-DPD (1) can be less complicated than that of a 2D-DPD (3). The advantage of 2D-DPD is its significantly lower sampling frequency compared with the WB-DPD. The PNS technique provides a solution to implement a low-complexity model at the low sampling rate.

The PNS reconstruction theorem for multi-band signal is presented in [20]. A high-rate signal is decimated using PNS of the third order [PNS(3)] as illustrated in Fig. 5 where we can split the samples into 3 channels: $s_1(n)$, $s_2(n)$ and $s_3(n)$ (sampled by pulses in blue, green and red, respectively) at a lower sampling rate f_s. These decimated samples have the same period T=1/f_s. According to the generalized sampling theory in [27], a bandlimited signal can be determined by L signals at sampling rate of $1/L$ of the Nyquist rate. A possible realization of this generalized sampling theory is the PNS reconstruction diagram as illustrated in Fig. 6. The block of $e^{j\omega d_l}$ represents a delay of d_l (l=0,..,L-1). The signals in the

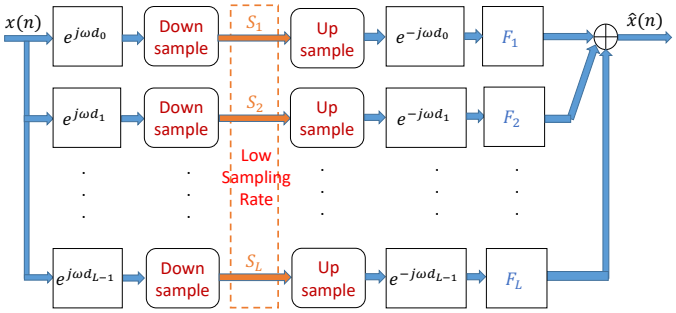

Fig. 6. Reconstruction of $x(n)$ using [PNS(L)].

dashed box are sampled at low rate. A multi-band-pass filter F_l is applied at the output of the l-th channel to enable that $x(n)$ can be reconstructed by summing up the decimated signals.

The details of solving [PNS(L)] reconstruction problem for multi-band signals have been given in [20]. To recall the part of this reconstruction technique which is used in our proposed DPD method, we first elaborate it using an example of [PNS(4)] reconstruction for a 4-band signal $x(n)$ with the bands evenly spaced. The spectrum of $x(n)$ is depicted as $X(f)$ in Fig. 4. The signal $X_i(f)$ (i=1,..,4) of the i-th band is centered at the carrier frequency f_i. With [PNS(4)], we decimate $x(n)$ to 4 channels of signals $s_1(n)$, $s_2(n)$, $s_3(n)$ and $s_4(n)$. The data samples $s_l(n)$ (l=1,..,4) has a delay d_{l-1} from $s_1(n)$, where d_0=0. The spectra $S_l(f)$ ($f \in$[-f_s/2,f_s/2]) of the decimated signal $s_l(n)$ has all $x(n)$ folded into a single frequency interval, which can be expressed as

$$\begin{aligned} S_l(f) =& X_1(f+f_1)e^{j2\pi f_1 d_{l-1}} + X_2(f+f_2)e^{j2\pi f_2 d_{l-1}} \\ &+X_3(f+f_3)e^{j2\pi f_3 d_{l-1}} + X_4(f+f_4)e^{j2\pi f_4 d_{l-1}}. \end{aligned} \quad (5)$$

where f_s are selected to have f_i as a multiple of f_s. If f_i is not a multiple of f_s, we can still find a solution, but the equations in following derivations will be more complex.

According to [20], the original $X(f)$ can be reconstructed at any frequency f by upsampling and summing up the decimated signals if $F_l(f)$ have solutions:

$$X(f) = \sum_{l=1}^{4} F_l(f) S_l(f + kf_s). \quad (6)$$

where k is an integer that $f+kf_s \in$[-f_s/2,f_s/2], and the filters $F_l(f)$ for reconstruction of a 4-band signal is a 4-band-pass filter whose frequency response has an identical shape as the spectrum of $X(f)$ in Fig. 4: in each band, $F_l(f)$ is flat, but the complex gains of $F_l(f)$ in these bands can be different:

$$F_l(f) = \sum_{i=1}^{4} A_l^{(i)} \text{rect}(\frac{f-f_i}{f_s}), \quad (7)$$

where rect(.) represents a rectangular function. The spectra of high rate signals upsampled from $s_l(n)$ are periodical duplicates of $S_l(f)$. According to (5)-(7), we can reconstruct the signal in the i-th band when $f \in$[-f_s/2+f_i,f_s/2+f_i] if (4) has a solution for $\boldsymbol{A}^{(i)}$, where $\boldsymbol{c}^{(i)}$ is a vector such that $c_i^{(i)}$=1 and $c_j^{(i)}$=0 (j=1,..,4, $j \neq i$). According to [20], the matrix $\boldsymbol{E}^{(i)}$ is non-singular if $(f_j$-$f_i)d_l$ is not an integer when j=1,..,4, $j \neq i$, l=1,..,4. We can then solve for $\boldsymbol{A}^{(i)}$.

Note that since the spectra of the decimated signal is duplicated in the entire band by upsampling, the PNS reconstruction is possible in any band whose center frequency is a multiple of f_s. The bands of reconstructed signal are selected by $F_l(f)$. We can obviously retrieve the baseband signals of X_i (i=1,...,4) separately without upsampling.

IV. Periodically Nonuniform Sampled DPD (PNS-DPD)

In this section, we propose a PNS-DPD which combines the advantages of the WB-DPD and the 2D-DPD: it can be implemented at the low sampling rate of the 2D-DPD while using the low-complexity model of the WB-DPD. We aim to process the dual-band signal as a single wide-band signal at low rate with aliasing effect, and then reconstruct the interested bands with PNS samples by solving (4) for $\boldsymbol{A}^{(i)}$.

A. Analysis of predistorted signal frequency components

The PNS reconstruction technique enables processing a high-rate signal with low-rate filters if they are placed in the dashed box in Fig. 6. In this paper, we aim to place DPD models in the dashed box. The reconstruction technique introduced in the previous section can be used to reconstruct the predistorted signals which enable PA linearization. Since DPD models are nonlinear, the predistorted signal always occupies wider band than the DPD input signal. For a dual-band input signal, its IMD products fall into some bands other than the transmission bands. Thus the predistorted wideband signal has more bands. In this section, we analyze the frequencies of these IMD products and explore an optimized PNS technique with knowledge of their frequencies.

First we make a simple analysis on frequency components of the WB-DPD output signal with help of (1). If we denote the signals of the lower band and the higher band by $u_L(n)$ and $u_H(n)$ in baseband respectively, the baseband DPD input is

$$u(n) = u_L(n)e^{-j2\pi f_g n} + u_H(n)e^{j2\pi f_g n}, \quad (8)$$

where $f_g = \frac{f_{p2}-f_{p1}}{2}$, f_{p1} and f_{p2} are RF carrier frequencies of the lower band and the higher band respectively. According

$$\underbrace{\begin{bmatrix} c_1^{(i)} \\ c_2^{(i)} \\ c_3^{(i)} \\ c_4^{(i)} \end{bmatrix}}_{\boldsymbol{c}^{(i)}} = \underbrace{\begin{bmatrix} 1 & e^{j2\pi(f_1-f_i)d_1} & e^{j2\pi(f_1-f_i)d_2} & e^{j2\pi(f_1-f_i)d_3} \\ 1 & e^{j2\pi(f_2-f_i)d_1} & e^{j2\pi(f_2-f_i)d_2} & e^{j2\pi(f_2-f_i)d_3} \\ 1 & e^{j2\pi(f_3-f_i)d_1} & e^{j2\pi(f_3-f_i)d_2} & e^{j2\pi(f_3-f_i)d_3} \\ 1 & e^{j2\pi(f_4-f_i)d_1} & e^{j2\pi(f_4-f_i)d_2} & e^{j2\pi(f_4-f_i)d_3} \end{bmatrix}}_{\boldsymbol{E}^{(i)}} \underbrace{\begin{bmatrix} A_1^{(i)} \\ A_2^{(i)} \\ A_3^{(i)} \\ A_4^{(i)} \end{bmatrix}}_{\boldsymbol{A}^{(i)}} \quad (4)$$

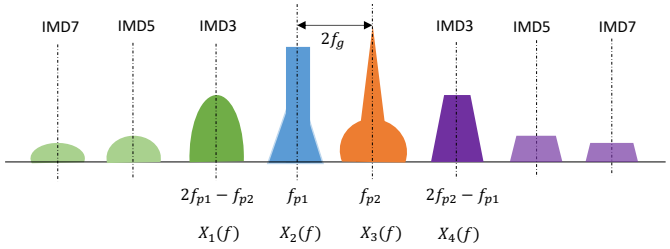

Fig. 7. Intermodulation created by WB-DPD for dual-band signal.

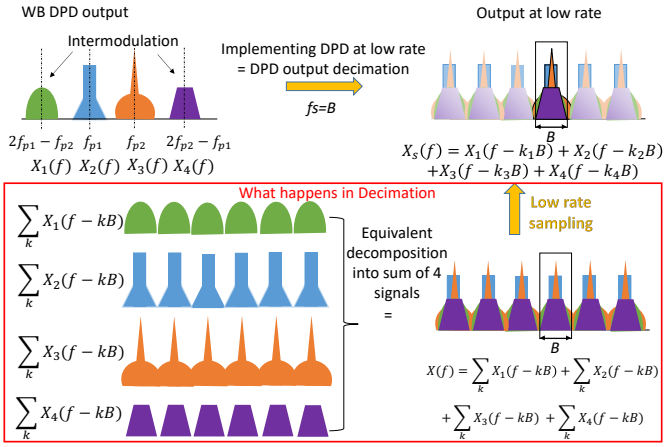

Fig. 8. Aliasing of different frequency components introduced in the proposed DPD implemented at low rate.

to (8) and (1), the DPD output is a function of the products between $u_L(n)$ and $u_H(n)$:

$$\begin{aligned} x(n) &= \sum_p \sum_q \sum_r \gamma_{pqr} u(n-q)|u(n-r)|^p \\ &= \sum_p \sum_q \sum_r \gamma_{pqr} \\ &\times (u_L(n-q)e^{-j2\pi f_g(n-q)} + u_H(n-q)e^{j2\pi f_g(n-q)}) \\ &\times |u_L(n-r)e^{-j2\pi f_g(n-r)} + u_H(n-r)e^{j2\pi f_g(n-r)}|^p, \end{aligned} \tag{9}$$

where q=r corresponds to the first branch of (1), $q < r$ and $q > r$ correspond to the second and the third branch of (1) respectively, γ_{pqr} are equivalent coefficients. Some frequency components other than $-f_g$ and f_g will be generated. For instance when p is even, we have

$$\begin{aligned} |u(n)|^p &= |(u_L(n)e^{-j2\pi f_g n} + u_H(n)e^{j2\pi f_g n})|^p \\ &= (u_L(n)e^{-j2\pi f_g n} + u_H(n)e^{j2\pi f_g n})^{\frac{p}{2}} \\ &\times (u_L^*(n)e^{j2\pi f_g n} + u_H^*(n)e^{-j2\pi f_g n}))^{\frac{p}{2}} \\ &= \sum_{p_1=0}^{\frac{p}{2}} \sum_{p_2=0}^{\frac{p}{2}} v(n) e^{j2\pi(2p_2-2p_1)f_g n} \end{aligned} \tag{10}$$

where $v(n) = u_L(n)^{p_1} u_L^*(n)^{\frac{p}{2}-p_1} u_H(n)^{p_2} u_H^*(n)^{\frac{p}{2}-p_2}$. According to (9) and (10), we can easily find out the distribution of $x(n)$ over frequency, which is located not only at $-f_g$ and f_g but also at $(2p_2-2p_1)f_g \pm f_g$, where $(p_1, p_2) \in [0, \frac{p}{2}]$ as illustrated in Fig. 7. The 3-rd order intermodulation (IMD3) is the most significant IMD [28]. In this paper, we consider only the IMD3 which is located at $\pm 3f_g$ in baseband. In RF domain the two IMD3 are located at $2f_{p1} - f_{p2}$ and $2f_{p2} - f_{p1}$ respectively as shown in Fig. 7. The predistorted signal is then an evenly spaced 4-band signal with similar spectral locations as in Fig. 4, where the signals in the bands are denoted $x_1(n)$, $x_2(n)$, $x_3(n)$ and $x_4(n)$. Their Fourier transforms are respectively $X_1(f)$, $X_2(f)$, $X_3(f)$, and $X_4(f)$, where $X_2(f)$ and $X_3(f)$ are desired signals to compensate for the PA distortion in transmission bands.

According to Nyquist sampling theorem, decimating a wide-band signal to a sampling rate smaller than its bandwidth will result in aliasing effects. Implementing the WB-DPD at a low sampling rate after proper adaptions on the model structure, e.g. the memory depth, will introduce a similar aliasing effect at the DPD output as depicted in Fig. 8. The decimation results in that the signals in occupied bands are shifted into an observation window with a bandwidth of f_s. Similar to (5), we have the baseband output signal of a WB-DPD model implemented at low rate as all its components folded up inside the small observation window $f \in$[-f_s/2,f_s/2]):

$$\begin{aligned} X_s(f) =& X_1(f-3f_g) + X_2(f-f_g) \\ &+X_3(f+f_g) + X_4(f+3f_g). \end{aligned} \tag{11}$$

With the PNS technique, the aliased signals $X_2(f)$ and $X_3(f)$ can be reconstructed with help of $X_s(f)$, so that the PA can be linearized in transmitting bands centered at f_{p1} and f_{p2} with a bandwidth f_s.

The PNS reconstruction technique presented in Section III is a general case for any values of d_l. In the case of predistorted signal for dual-band transmission, we noticed the symmetry of the frequencies of X_1 and X_4. Thus, if d_1 and d_2 allow $-2\pi 3 f_g d_l$=$2\pi 3 f_g d_l + 2k\pi$ (l=1,2) where k is an integer, and d_3=0, we can solve (4) with $A_4^{(i)}$=0, which removes the sample channel S_4 and reduces 1/4 of the complexity. Thus we have $d_l = k/(6f_g)$. Note that if k is a multiple of 3, $\boldsymbol{E}^{(i)}$ is singular. We should keep (k mod 3)$\neq$ 0. In this paper, we choose $d_1 = 1/(6f_g)$ and $d_2 = 1/(3f_g)$.

B. PNS-DPD structure

Our purpose is to reconstruct the desired predistorted signals (signals X_2 and X_3 in Fig. 7 and in (11)) at the PA input as illustrated in Fig. 9. We propose a PNS-DPD as the dual-input and dual-output block depicted in Fig. 10.

The diagram of the proposed PNS-DPD is depicted in Fig. 11. An identical single-input single-output (SISO) DPD model is implemented in three channels separately. The signals $u_L(n)$ and $u_H(n)$ are folded with aliasing for inputs of SISO DPDs:

$$\begin{aligned} u_s(n) &= u_L(n) + u_H(n), \\ u_{a_l}(n) &= u_{L,d_l}(n)e^{-j2\pi f_g d_l} + u_{H,d_l}(n)e^{j2\pi f_g d_l}, \end{aligned} \tag{12}$$

where $l \in [1,2]$, d_1=$1/(6f_g)$ and d_2=$1/(3f_g)$, $u_{L,d_l}(n)$ and $u_{H,d_l}(n)$ are $u_L(n)$ and $u_H(n)$ delayed for d_l by delay adjust filters (DAF) as designed in [19] respectively. This generates the aliased predistorted signal x_s in (11), and 2 auxiliary predistorted signals x_{a1} and x_{a2}, which play the roles of s_1, s_2 and s_3 in Section III respectively. The DAF ($-d_l$) behind

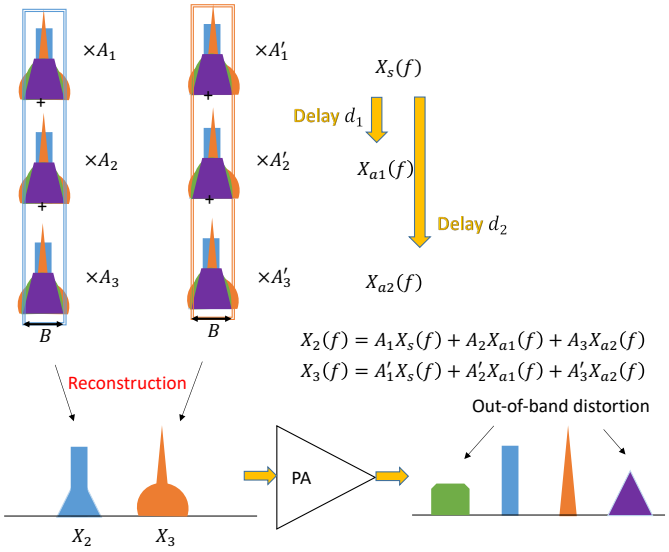

Fig. 9. Reconstruction of predistorted signal.

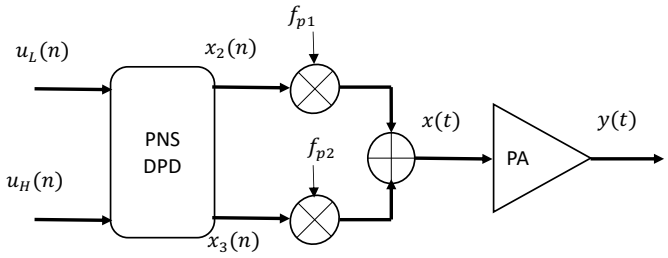

Fig. 10. The structure of the DPD and PA system.

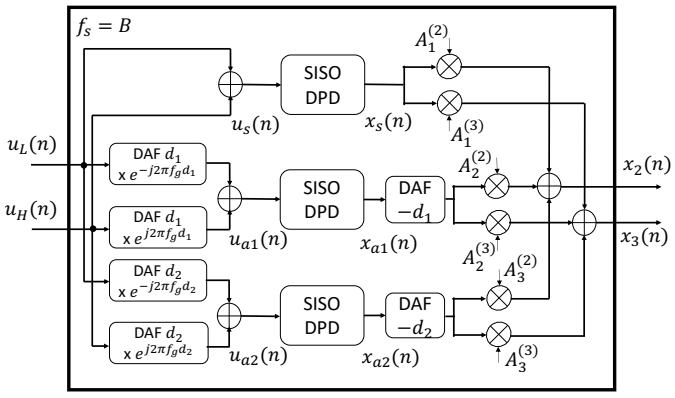

Fig. 11. The structure of the proposed 2D-PNS-DPD.

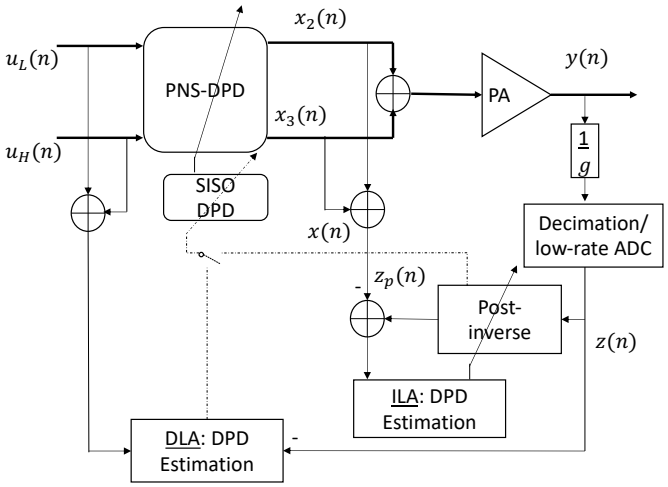

Fig. 12. Identification of PNS-DPD model using direct and indirect learning architecture (DLA/ILA).

the DPD model are used to compensate for the delay of d_l in the l-th auxiliary channel. The three SISO DPD outputs are multiplied by $\boldsymbol{A}^{(2)}$ and $\boldsymbol{A}^{(3)}$ to reconstruct the predistorted signals X_2 and X_3, respectively. These predistorted signals are then modulated to their frequency carriers and are fed to the PA as illustrated in Fig. 10.

The values of $\boldsymbol{A}^{(2)}$ and $\boldsymbol{A}^{(3)}$ are pre-calculated as solutions to (4) for the 2nd and 3rd bands respectively, which are independent of the transmitted signals. Thus they do not bring any computational burden.

There are three channels of signal to be processed but the SISO DPD model is identical for each channel. Thus only one single feedback path is needed for model identification. The model coefficients can be estimated using DLA or ILA as in Fig. 12. This is the same procedure as high-rate WB-DPD in Fig. 2 with decimated PA output $y(n)$. The decimated PA input is equal to the sum of two outputs of PNS-DPD $x_2(n)$ and $x_3(n)$ in ILA so that we replace $\boldsymbol{x}$ in (2) by

$$\boldsymbol{x} = \boldsymbol{x_2} + \boldsymbol{x_3}. \tag{13}$$

Since the SISO DPD output should contain the information of both transmitted signal and IMDs as illustrated in Fig. 8, the signals used for SISO model identification are sampled at the same rate as the DPD sampling rate and should be aliased without any filtering. One solution is to acquire the PA output signal $y(n)$ directly with a low-rate ADC as in [29]. The aliased IMD information helps to correctly identify the nonlinearities of the SISO model in the PNS-DPD.

The PNS-DPD is based on signal processing techniques which is not limited by the behavioral models. The complexity is reduced thanks to the reduction of the number of model inputs and the number of reconstruction channels. Therefore, any model pruning technique can be applied along with the proposed PNS-DPD for further complexity reduction.

V. Experimental Results

A. Test bench

We use test bench of WebLab [21] for measurements as depicted in Fig. 13.

The baseband IQ signal is fed from the PC Workstation to the driver through a Vector Signal Transceiver (PXIe-5646R VST) using a 200 MHz sampling frequency. The VST up-converts the baseband signal to the carrier frequency 2.14 GHz. The signal at the output of the PA is then down-converted to baseband by the VST which provides to the PC workstation the baseband signal digitized with a sampling frequency of 200 MHz. The input and output baseband signals are then synchronized in time to be used by the identification algorithm (2).

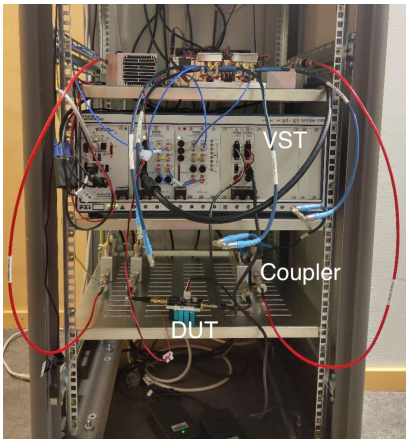

Fig. 13. Test bench of WebLab [21] for Experimental Implementation.

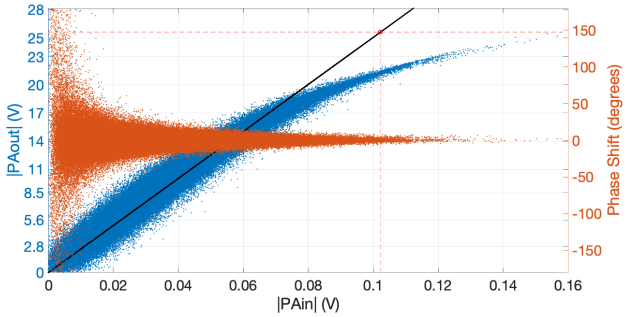

Fig. 14. PA AMAM & AMPM curves for dual band 5 MHz LTE signal.

A GaN PA CGH40006P transistor mounted in the manufacturer demo-board fabricated by CREE has been used to validate the proposed low rate DPD. Its nominal gain is 13 dB at 2 GHz and the output power at 1dB gain compression is 40.2 dBm.

The nonlinearities and the memory effect of this PA can be seen from the AM/AM & AM/PM (Amplitude Modulation/Amplitude Modulation & Amplitude Modulation/Phase Modulation) curves in Fig 14 in the case the stimulus is a dual-band 5 MHz LTE signal with 40 MHz frequency separation. The average power of the signal at the input of the driver is around -26.32 dBm. The measured average output power of the PA is 29.73 dBm.

In order to evaluate the proposed low rate DPD, we take the original signal at rate of 200 MHz as high rate signal. A decimation to low rate is applied before feeding the signals to the DPD. Two tests have been implemented in this section to validate the proposed PNS-DPD:

- Test I: stimulus is a dual-band 5 MHz LTE signal with 40 MHz frequency separation, PNS-DPD is implemented at 20 MHz.
- Test II: stimulus is a dual-band 5 MHz LTE signal with 60 MHz frequency separation, PNS-DPD is implemented at 15 MHz.

Wideband DPD and 2D-DPD are tested as references in comparison. The wideband DPD is implemented at 200 MHz which is fixed by WebLab configuration. The 2D-DPD is implemented at the same rate as the PNS-DPD.

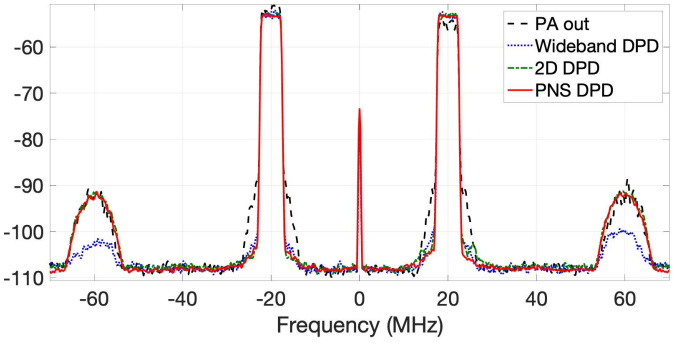

Fig. 15. PA output spectra with different DPD approaches for dual-band 5 MHz LTE: Test I.

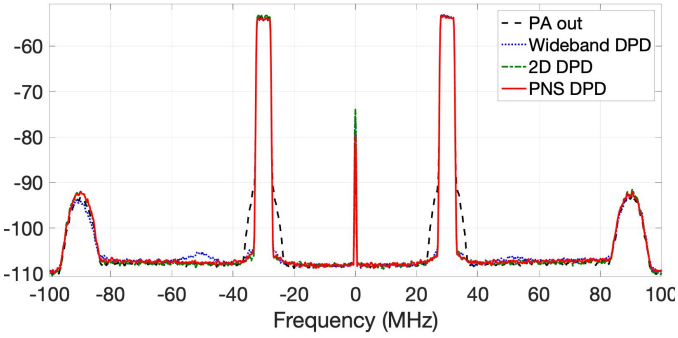

Fig. 16. PA output spectra with different DPD approaches for dual-band 5 MHz LTE: Test II.

The tests are iterative: we take a segment of 500 000 samples of high rate signal and divide it equally into 5 segments for a 5-iteration test. In each iteration, 100 000 samples of high rate signal are decimated to low rate signal (e.g. 10 000 samples in Test I) and then are fed to the DPD. The computed predistorted signal is then up-converted to 200 MHz sampling rate and is fed to WebLab testbench. The observed PA output is then decimated to low rate for DPD model identification. The estimated DPD coefficients are updated for the test of the following iteration with a low rate signal which is decimated from another 100 000 samples high rate signal. The DPD coefficients are updated using Gaussian-Newton method which takes consideration of their values at the former iteration.

B. Linearization performance of the proposed DPD

The output spectra of the PA linearized by different DPD approaches in Test I and II are illustrated in Fig. 15 and Fig. 16 respectively. The PA output without linearization is shown by dotted curve. The linearization performance of conventional high-rate WB-DPD is shown by dashed curve. The spectra of the proposed 2D-DPD linearization is shown by dash-dotted curve. And the spectra of conventional PNS-DPD linearization is shown by straight curve. The adjacent channel power ratio (ACPR) and error vector magnitude (EVM) are given as well as the sampling rate of DPD implementation procedure and DPD identification procedure of Test I and II in Table II and Table III respectively. The AMAM & AMPM curves of Band

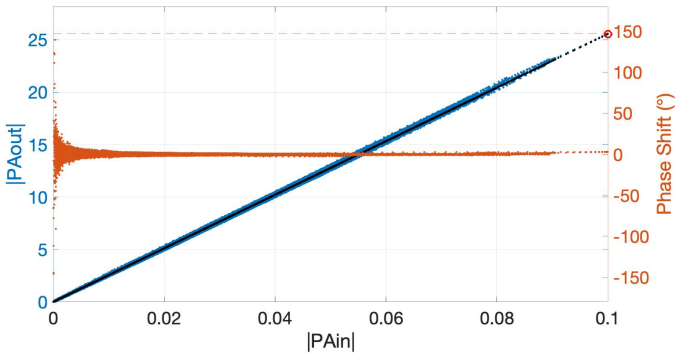

Fig. 17. AMAM & AMPM curves of Band 1 after linearization by PNS-DPD.

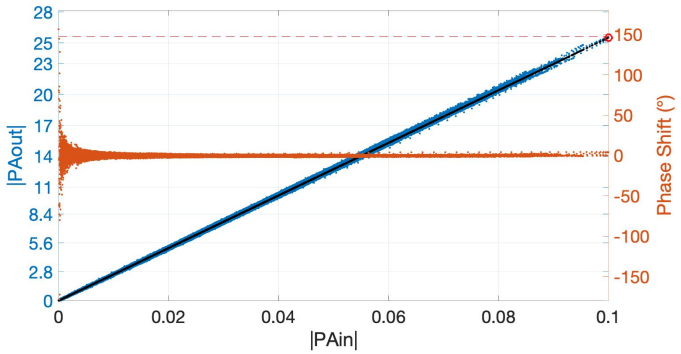

Fig. 18. AMAM & AMPM curves of Band 2 after linearization by PNS-DPD.

1 and Band 2 after linearization by PNS-DPD are depicted in Fig. 17 and Fig. 18 respectively.

The optimal model structures for the DPD approaches are determined using the algorithm proposed in [30]. The model structure for the conventional WB-DPD (1) is

$$\begin{aligned} \mathcal{K}_a =& 6, \mathcal{L}_a = 3 \\ \mathcal{K}_b =& 1, \mathcal{L}_b = 1, \mathcal{M}_b = 1 \\ \mathcal{K}_c =& 1, \mathcal{L}_c = 7, \mathcal{M}_c = 2. \end{aligned} \tag{14}$$

There are 33 coefficients.

The model structure for the proposed PNS-DPD (1) is

$$\begin{aligned} \mathcal{K}_a =& 5, \mathcal{L}_a = 3 \\ \mathcal{K}_b =& 0 \\ \mathcal{K}_c =& 1, \mathcal{L}_c = 2, \mathcal{M}_c = 2. \end{aligned} \tag{15}$$

There are 19 coefficients. The number of coefficients is reduced because the model is run at low rate, which needs less memory taps.

The model structure for the conventional 2D-DPD (3) is

$$\begin{aligned} \mathcal{K}_a =& 5, \mathcal{L}_a = 3 \\ \mathcal{K}_b =& 2, \mathcal{L}_b = 3, \mathcal{M}_b = 1 \\ \mathcal{K}_c =& 1, \mathcal{L}_c = 4, \mathcal{M}_c = 2. \end{aligned} \tag{16}$$

There are 76 coefficients for each sub-DPD.

The proposed PNS-DPD reaches the same level with the conventional WB-DPD and 2D-DPD as depicted in Fig. 15 and Fig. 16. It is shown in Table II that in Test I the proposed

TABLE I
NUMBER OF FLOPS FOR OPERATIONS

Operation	FLOPs	Operation	FLOPs
Real Addition	1	Real Multiplication	1
Real Division	4	Complex Addition	2
Complex Multiplication	6	Complex-Real Multiplication	2
Square-root	6~8		

TABLE II
LINEARIZATION PERFORMANCE OF DIFFERENT DPD APPROACHES: TEST I

		No DPD	WB DPD	PNS DPD	2D DPD
Impl. rate (MHz)		-	200	20	20
Nb of Coefficients		-	33	19	76
Nb of channels		-	1	3	2
C_{impl}		-	56800	15480	26160
Band 1	ACPR.L (dBc)	-40.1	-47.7	-49.3	-49.6
	ACPR.H (dBc)	-39.5	-47.6	-48.7	-47.0
	EVM (%)	5	0.9	0.9	1.1
Band 2	ACPR.L (dBc)	-37.4	-46.9	-47.6	-47.2
	ACPR.H (dBc)	-36.7	-47.1	-49.2	-46.6
	EVM (%)	5	1.1	1.2	1.4
Iden. rate (MHz)		-	200	20	20
Iden. channels		-	1	1	2
C_{iden}		-	1089	361	11552

Impl. : Implementation
Iden. : Identification

PNS-DPD achieves better ACPR and EVM compared with conventional approaches.

The conventional WB-DPD needs over 10 times higher sampling rate in implementation and identification procedures compared with the proposed PNS-DPD and the conventional 2D-DPD. In terms of model complexity, the proposed PNS-DPD has the lowest number of coefficients. We estimate the complexity of DPD implementation by

$$C_{\text{impl}} = f_s \cdot \text{flops} \cdot S_{\text{impl}} \tag{17}$$

where f_s is the sampling rate, flops is the number of flops (floating point operation per sample) in DPD computation, S_{impl} is the number of channels in implementation. The calculation of flops is based on Table I in [22]. For the single-band GMP model in WB-DPD and PNS-DPD, the number of flops is:

$$\text{flops} = 3 + 7 + 2\mathcal{K}_a + 2\mathcal{K}_b\mathcal{M}_b + 2\mathcal{K}_c\mathcal{M}_c + 8R - 2; \tag{18}$$

where R is the number of coefficients of the GMP model. For the DAFs in Fig. 11, an N-tap fractional delay filter needs the number of flops is $8N$-2. In this paper we implement with 5 taps for all DAFs, which results in 228 additional flops. The complexity of the proposed PNS-DPD also includes 6 complex complications of $\boldsymbol{A}^{(2)}$ and $\boldsymbol{A}^{(3)}$, which needs 36 flops. For the dual-band GMP model in (3), the number of flops is:

$$\begin{aligned} \text{flops} = 3 + 7 + \mathcal{K}_a(\mathcal{K}_a + 1) + \mathcal{K}_b(\mathcal{K}_b + 1)\mathcal{M}_b \\ + \mathcal{K}_c(\mathcal{K}_c + 1)\mathcal{M}_c + 8R - 2. \end{aligned} \tag{19}$$

The complexity of DPD identification can be given in a similar way according to [31]

$$C_{\text{iden}} = R^2 \cdot S_{\text{iden}} \tag{20}$$

where S_{iden} is the number of channels in implementation.

TABLE III
LINEARIZATION PERFORMANCE OF DIFFERENT DPD APPROACHES: TEST II

		No DPD	WB DPD	PNS DPD	2D DPD
Impl. rate (MHz)		-	200	15	15
Nb of Coefficients		-	33	19	76
Nb of channels		-	1	3	2
C_{impl}		-	56800	11610	19620
Band 1	ACPR.L (dBc)	-39.2	-51.7	-52.2	-52.1
	ACPR.H (dBc)	-39.7	-52.2	-52.4	-52.1
	EVM (%)	5	1.1	1.1	1.0
Band 2	ACPR.L (dBc)	-39.2	-53.0	-52.9	-53.0
	ACPR.H (dBc)	-38.9	-52.6	-52.7	-52.6
	EVM (%)	5	1.1	1.1	1.0

Impl. : Implementation
Iden. : Identification

According to Table II and Table III, the proposed PNS-DPD has advantages on complexities of both DPD implementation and DPD identification in both Test I and II. The implementation complexity of PNS-DPD is about 20% of the WB-DPD and 60% of the conventional 2D-DPD. The identification complexity of PNS-DPD is about 3 times lower than WB-DPD and about 30 times lower than the conventional 2D-DPD. The combined advantages of the proposed PNS-DPD on sampling rate and model complexity have been confirmed with the experimental results by reaching the same linearization performance as conventional methods.

C. Discussion

The IMD3 is the strongest IMD. The other IMDs such as IMD5 and IMD7 are usually in low power with negligible influence. In case of the DPD model with stronger nonlinearity (e.g. $\mathcal{K} > 7$), the power IMD5 may grow up and the proposed model needs to consider the 6-band case (2 transmitted bands, 2 IMD3, 2 IMD5) in (4). With the same idea of utilizing the symmetry of frequency locations of these bands, we need to add a 4-th branch in Fig. 11. This will increase the complexity by 1/3. But compared with the 2D-DPD whose complexity is in order of $\mathcal{O}(\mathcal{K}^2)$, the proposed PNS-DPD will have larger advantage on complexity when the nonlinearity gets stronger.

The proposed PNS-DPD technique can also be generalized to multi-dimensional cases with more than 2 bands. In this paper, we have demonstrated that the PNS-DPD outperforms the 2D-DPD model on complexity because the 2D-DPD has many basis functions to represent the IMDs between the signals two bands. Obviously we can foresee that an MD-DPD with M>2 have much more complicated IMDs. The complexity of the PNS-DPD mainly depends on the number of channels which is related to the number of bands of the predistorted wideband signal. In the case that these IMDs fall into the transmission bands, especially when transmission bands are evenly spaced in frequency, the PNS-DPD will have an enormous advantage on the model complexity.

VI. CONCLUSION

In this paper, we proposed a novel PNS-DPD for concurrent dual-band transmitter linearization. This approach exhibits good linearization performance while outperforming the conventional methods on complexities of DPD implementation for a factor of over 2 and DPD identification for a factor of over 3. A low-complexity model can be used as the DPD and can be implemented at the same sampling rate as the conventional 2D-DPD thanks to the proposed PNS technique, which has combined advantages on both sampling rate and model complexity. The proposed DPD needs only one feedback path for identification without any additional processing.

ACKNOWLEDGMENT

This work was performed within the strategic innovation program Smarter Electronic Systems – a joint program by Vinnova, the Swedish research council Formas and the Swedish Energy Agency – together with Chalmers, Ericsson and Bluetest.

REFERENCES

[1] K. Samdanis and T. Taleb, "The road beyond 5G: A vision and insight of the key technologies," *IEEE Network*, pp. 1–7, 2020.
[2] E. G. Larsson, O. Edfors, F. Tufvesson, and T. L. Marzetta, "Massive mimo for next generation wireless systems," *IEEE IEEE Commun. Mag.*, vol. 52, no. 2, pp. 186–195, February 2014.
[3] A. Katz, J. Wood, and D. Chokola, "The evolution of PA linearization: From classic feedforward and feedback through analog and digital predistortion," *IEEE Microw. Mag.*, vol. 17, no. 2, pp. 32–40, Feb 2016.
[4] J. Kim and K. Konstantinou, "Digital predistortion of wideband signals based on power amplifier model with memory," *Electronics Letters*, vol. 37, no. 23, pp. 1417–1418, Nov 2001.
[5] D. Morgan, Z. Ma, J. Kim, M. Zierdt, and J. Pastalan, "A generalized memory polynomial model for digital predistortion of RF power amplifiers," *IEEE Trans. Signal Process.*, vol. 54, no. 10, pp. 3852–3860, Oct. 2006.
[6] A. Zhu, J. Pedro, and T. Brazil, "Dynamic deviation reduction-based volterra behavioral modeling of RF power amplifiers," *IEEE Trans. Microw. Theory Techn.*, vol. 54, no. 12, pp. 4323–4332, Dec 2006.
[7] A. Zhu, "Decomposed vector rotation-based behavioral modeling for digital predistortion of RF power amplifiers," *IEEE Trans. Microw. Theory Techn.*, vol. 63, no. 2, pp. 737–744, Feb 2015.
[8] S. Wang, M. Abi Hussein, O. Venard, and G. Baudoin, "Optimal sizing of two-stage cascaded sparse memory polynomial model for high power amplifiers linearization," *IEEE Trans. Microw. Theory Techn.*, vol. 66, no. 9, pp. 3958–3965, Sep. 2018.
[9] J. Wood, "System-level design considerations for digital pre-distortion of wireless base station transmitters," *IEEE Trans. Microw. Theory Techn.*, vol. 65, no. 5, pp. 1880–1890, May 2017.
[10] R. Jevtic and C. Carreras, "Power estimation of embedded multiplier blocks in fpgas," *IEEE Trans. Very Large Scale Integr. (VLSI) Syst.*, vol. 18, no. 5, pp. 835–839, May 2010.
[11] P. Roblin, C. Quindroit, N. Naraharisetti, S. Gheitanchi, and M. Fitton, "Concurrent linearization: The state of the art for modeling and linearization of multiband power amplifiers," *IEEE Microw. Mag.*, vol. 14, no. 7, pp. 75–91, Nov 2013.
[12] S. Bassam, M. Helaoui, and F. Ghannouchi, "2-D digital predistortion (2-D-DPD) architecture for concurrent dual-band transmitters," *IEEE Trans. Microw. Theory Techn.*, vol. 59, no. 10, pp. 2547 –2553, oct. 2011.
[13] M. Cabarkapa, N. Neskovic, and D. Budimir, "A generalized 2-D linearity enhancement architecture for concurrent dual-band wireless transmitters," *IEEE Trans. Microw. Theory Techn.*, vol. 61, no. 12, pp. 4579–4590, 2013.
[14] B. Fehri and S. Boumaiza, "Baseband equivalent volterra series for digital predistortion of dual-band power amplifiers," *IEEE Trans. Microw. Theory Techn.*, vol. 62, no. 3, pp. 700–714, 2014.
[15] N. Kelly, W. Cao, and A. Zhu, "Preparing linearity and efficiency for 5G: Digital predistortion for dual-band doherty power amplifiers with mixed-mode carrier aggregation," *IEEE Microw. Mag.*, vol. 18, no. 1, pp. 76–84, Jan 2017.

[16] A. Kohlenberg, "Exact interpolation of band-limited functions," *J. Appl. Phys.*, vol. 24, no. 12, pp. 1432–1436, Dec. 1953.

[17] D. Schwingshackl and G. Kubin, "Polyphase representation of multirate nonlinear filters and its applications," *IEEE Trans. Signal Process.*, vol. 55, no. 5, pp. 2145–2157, 2007.

[18] T. Gotthans, R. Marsalek, and J. Gotthans, "Wideband digital predistortion with sub-nyquist nonuniform sampling and reconstruction of feedback path," in *2017 IEEE Top. Conf. RF/Microw. Power Amplif. Radio Wirel. Appl. (PAWR)*, 2017, pp. 70–72.

[19] Y. Li, X. Wang, and A. Zhu, "Sampling rate reduction for digital predistortion of broadband RF power amplifiers," *IEEE Trans. Microw. Theory Techn.*, pp. 1–11, 2019.

[20] Yuan-Pei Lin and P. P. Vaidyanathan, "Periodically nonuniform sampling of bandpass signals," *IEEE Trans. Circuits Syst. II. Analog Digit. Signal Process.*, vol. 45, no. 3, pp. 340–351, Mar. 1998.

[21] P. N. Landin, S. Gustafsson, C. Fager, and T. Eriksson, "Weblab: A web-based setup for PA digital predistortion and characterization [application notes]," *IEEE Microw. Mag.*, vol. 16, no. 1, pp. 138–140, Feb 2015.

[22] A. S. Tehrani, H. Cao, S. Afsardoost, T. Eriksson, M. Isaksson, and C. Fager, "A comparative analysis of the complexity/accuracy tradeoff in power amplifier behavioral models," *IEEE Trans. Microw. Theory Techn.*, vol. 58, no. 6, pp. 1510–1520, June 2010.

[23] C. Kantana, O. Venard, and G. Baudoin, "Comparison of GMP and DVR models," in *Proc. 2018 Int. Workshop Integr. Nonlinear Microw. Millimetre-Wave Circuits (INMMIC)*, Jul. 2018, pp. 1–3.

[24] M. Abi Hussein, V. Bohara, and O. Venard, "On the system level convergence of ila and dla for digital predistortion," in *2012 Int. Symp. Wireless Commun. Syst. (ISWCS)*, Aug 2012, pp. 870–874.

[25] S. Wang, M. Abi Hussein, O. Venard, and G. Baudoin, "Impact of the normalization gain of digital predistortion on linearization performance and power added efficiency of the linearized power amplifier," in *2017 12th Eur. Microw. Integr. Circuits Conf. (EuMIC)*, Oct. 2017, pp. 310–313.

[26] C. Eun and E. Powers, "A new volterra predistorter based on the indirect learning architecture," *IEEE Trans. Signal Process. on*, vol. 45, no. 1, pp. 223–227, Jan 1997.

[27] A. Papoulis, "Generalized sampling expansion," *IEEE Trans. Circuits Syst*, vol. 24, no. 11, pp. 652–654, 1977.

[28] J. Wood, *Behavioral Modeling and Linearization of RF Power Amplifiers:*, ser. Artech House Microwave Library. Artech House, 2014.

[29] Z. Wang, L. Guan, and R. Farrell, "Undersampling observation-based compact digital predistortion for single-chain multiband and wideband direct-to-rf transmitter," *IEEE Trans. Microw. Theory Techn.*, vol. 65, no. 12, pp. 5274–5283, Dec 2017.

[30] S. Wang, M. Abi Hussein, O. Venard, and G. Baudoin, "A novel algorithm for determining the structure of digital predistortion models," *IEEE Trans. Veh. Technol.*, vol. 67, no. 8, pp. 7326–7340, Aug. 2018.

[31] S. Wang, M. Abi Hussein, O. Venard, and G. Baudoin, "Performance analysis of multi-stage cascaded digital predistortion," in *2017 40th Int. Conf. Telecommun. and Signal Process. (TSP)*, Jul. 2017, pp. 275–248.

Siqi Wang received the B.S. degree from Huazhong University of Science and Technology, Wuhan, China in 2012, the M.S. degree from the University of Paris-Sud, Orsay, France in 2014, and the Ph.D. degree from the University of Paris-Est Marne La Vallée, Champs sur Marne, France, in 2018. He has been a researcher fellow with GeePs, Centrale-supélec in 2018-2019. He is currently a researcher fellow with Chalmers University of Technology since 2019. His research interests include wireless communications, digital predistortion, neural networks, energy efficiency optimization for wireless communication systems.

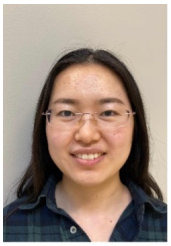

Wenhui Cao (S?15) received the B.E. degree in automation from the Beijing University of Chemical Technology, Beijing, China, in 2013, and the Ph.D. degree in electronic engineering from University College Dublin (UCD), Dublin, Ireland, in 2017. From 2013 to 2017, she was with the RF and Microwave Research Group, UCD. She was a Postdoc in Chalmers University of Technology from 2019 to 2020. Her research interests include nonlinear behavioral modelling and linearization of RF power amplifiers, digital post-correction of high-speed ADCs, digital suppression of TX-induced interference in FDD transceiver, and high-performance field-programmable gate-array (FPGA) implementation methodologies. She is currently a Radio system designer in Ericsson, Sweden.

Rui Hou (S?12?M?18) received the M.S. degree in microelectronics and the Ph.D. degree in electrical engineering from the Delft University of Technology, Delft, The Netherlands, in 2008 and 2017, respectively. From 2008 to 2011, he was with the Space Research Institute of the Netherlands, Utrecht, The Netherlands. Since 2015, he has been with Ericsson AB, Stockholm, Sweden, where he is currently the Senior Specialist in RF Technology.

Thomas Eriksson received the Ph.D. degree in Information Theory from Chalmers University of Technology, Gothenburg, Sweden, in 1996. From 1990 to 1996, he was at Chalmers. In 1997 and 1998, he was at AT&T Labs - Research, Murray Hill, NJ, USA. In 1998 and 1999, he was at Ericsson Radio Systems AB, Kista, Sweden. Since 1999, he has been with Chalmers University, where he is currently a professor of communication systems. Further, he was a guest professor with Yonsei University, S. Korea, in 2003-2004. He has authored or co-authored more than 300 journal and conference papers, and holds 14 patents. Prof. Eriksson is leading the research on hardware-constrained communications with Chalmers University of Technology. His research interests include communication, data compression, and modeling and compensation of non-ideal hardware components (e.g. amplifiers, oscillators, and modulators in communication transmitters and receivers, including massive MIMO). Currently, he is leading several projects on e.g. 1) massive MIMO communications with imperfect hardware, 2) wideband linearization (DPD), 3) Efficient and linear transceivers, etc. He is currently the Vice Head of the Department of Signals and Systems with Chalmers University of Technology, where he is responsible for undergraduate and master¥s education.